JAST, Vol. 5, No. 1, pp 1–11

JAST
Journal of Aerospace Science and Technology

Numerical Analysis of MAV's Flapping Wings in Unsteady Conditions

R. Kamali[1], S. Rezaei Ravesh[2]

Today, Flapping Micro Aerial Vehicles (MAV) are used in many different applications. Reynolds Number for this kind of aerial vehicle is about $10^4 \sim 10^5$, which shows dominancy of inertial effects in comparison to viscous effects in the flow field in areas except adjacent to the solid boundaries. Because of the periodic flapping stroke, fluid flow is unsteady. In addition, these creatures have some complexities in kinematic modeling. Although numerical methods are widely used for unsteady aerodynamic problems, it is highly difficult to solve the full 3D Navier–Stokes equations for complex flows like the ones for the flapping insect wings. Actually, the numerical simulation of flapping wings for different conditions of flapping frequencies and wing shapes has not been done yet. Thus, the present study is a pioneer. In this work, a computer code based on the unsteady Panel Method has been developed for the flow analysis. The prepared algorithm and the computer code are capable of modeling MAV's flapping wings in different unsteady conditions. The results of the aerodynamic design coefficients have been drawn. At the end the optimum wing shape and flapping frequency are discussed as other findings of this study.

INTRODUCTION

Flapping wing flight stands out as one of the most complex yet widespread modes of transportation found in nature. Over a million different species of insects fly with flapping wings, and 10,000 types of birds and bats flap their wings for locomotion [1]. Flapping wing designs are subject of great interest by the scientific community, as their capability for complex motion is thought to hold great potential for the exploitation of unsteady aerodynamic effects. For practical use in the conceptual and preliminary design of flapping wing vehicles, an efficient and easy-to-use tool providing estimates of aerodynamic forces and moment coefficients would be of great benefit. Such a tool would allow selection of design variables through trade studies, and can be used in conjunction with optimization algorithms without a considerable time investment.

The studies on flapping motion flight can be classified into two main parts: the zoological configurations and the simplified configurations. The zoological configurations are performed based on the study of insects or birds [2]. The simplified configurations are mostly the works based on the aerodynamics of the flow. The models are made easier such that the real insect/bird wing geometries are replaced with different pre-defined aerodynamic profiles. Although numerical methods are widely used for unsteady aerodynamic problems, it is highly difficult to solve the full 3D Navier–Stokes equations for complex flows like the ones of the flapping insect wings. Hamdani and Sun [3] simulated a series of impulsive starts at different accelerations around a 2D insect wing. The mean streamwise velocity field of the wake of a NACA 0012 airfoil oscillating in plunge at zero free stream velocity and at a zero angle of incidence at the neutral position was calculated by Lai and Platzer [4]. Wang *et.al.* [5] also performed a complete study on sinusoidal flapping motion in hover mode by giving a comparison of two-dimensional numerical simulations using an elliptical cross section with three-dimensional experimental results. They also presented comparisons of computational, experimental and quasi-steady forces and examined unsteady effects such as wing acceleration and wake capture mechanism.

Dickinson [6] experimentally observed that four important parameters of stroke reversal influence the

1. *Assistant Professor, Dept. of Mech. Eng., Shiraz Univ., Shiraz, Iran, Email: rkamali@shirazu.ac.ir.*
2. *MSc Student, Dept. of Mech. Eng., Shiraz Univ., Shiraz, Iran.*

generation of the force during the subsequent stroke namely the position of the rotational axis, the speed of rotation, the angle of attack of the preceding stroke and the length of the preceding stroke. The motion of the wing profile was divided into three temporally distinct phases: the first translation (downstroke), wing rotation, and the second translation in the opposite direction from the first (upstroke).

The most efficient computational tool among conventional methods such as momentum, blade-element, hybrid momentum (or vortex), lifting-line, two-dimensional thin aerofoil, lifting surface (or vortex lattice) and panel method, is the last one [7]. The unsteady aerodynamic Panel Method is a classical boundary element method which relies on developing a distribution of source and doublet singularities on wing surface and doublet singularities on the wake. This method is based on the potential theory which assumes inviscid flow.

The unsteady panel method is valid for Reynold's number of order 10^4 and above (Re= cU/ν , where c is nominal chord length, U is based on the flapping frequency, a nominal radius, as well as the free-stream velocity; ν is the kinematic viscosity). Some advantages such as, accommodation of the detailing of the trailing wake, inclusion of the dynamic effects and simple kinematic modeling, make panel method adequate for analysis of the flapping wings.

DEFINITION OF THE FLAPPING MOTION

In the present study, the flapping motion is studied for the wings which use a NACA airfoil. The flapping motion is composed using the superposition of a translational motion and a rotational motion around a center of rotation. As shown in Figure 1, the flapping motion is divided into four regions with the first region corresponding to the first half of the upstroke and the second region representing the first half of the downstroke. The third and fourth regions are the mirror images of these two regions, corresponding to the second half of the downstroke as well as the upstroke, respectively. This motion obeys a sinusoidal flapping pattern. During the different phases ($0 < \phi_x < 2\pi$), the orientation of the wing spanwise axis is changed. This makes the amplitude of flapping different for the points on the wing surface. If Z_i shows z-coordinate of any point of the wing with amplitude A_i, we have,

$$Z_i = A_i \sin(\omega_x t) = A_i \sin(\phi_x) \tag{1}$$

$$\dot{Z}_i = A_i \omega_x \cos(\omega_x t) = A_i \omega_x \cos(\phi_x) \tag{2}$$

where ω_x is the flapping frequency. To simplify the calculations, $\omega_x t$ is replaced by ϕ_x, which shows a quasi-steady flapping while the kinematic of motion is unsteady.

BASIC EQUATIONS AND NUMERICAL SCHEMES

As shown in Figure 2, to kinematically model the problem, we consider two frames of reference: an inertial frame (X, Y, Z) and a non-inertial body's frame (x, y, z).

The fluid surrounding the body is assumed to be inviscid, irrotational and incompressible over the entire flow field, excluding the body's solid boundaries and its wakes. Therefore, a velocity potential $\Phi(X, Y, Z)$ can be defined in the inertial frame and the continuity equation in this frame of reference becomes:

$$\nabla^2 \Phi = 0 \tag{3}$$

The first boundary condition requiring zero normal velocity across the body's solid boundaries is:

$$(\vec{\nabla}\Phi + \vec{V}) \cdot \vec{n} = 0 \tag{4}$$

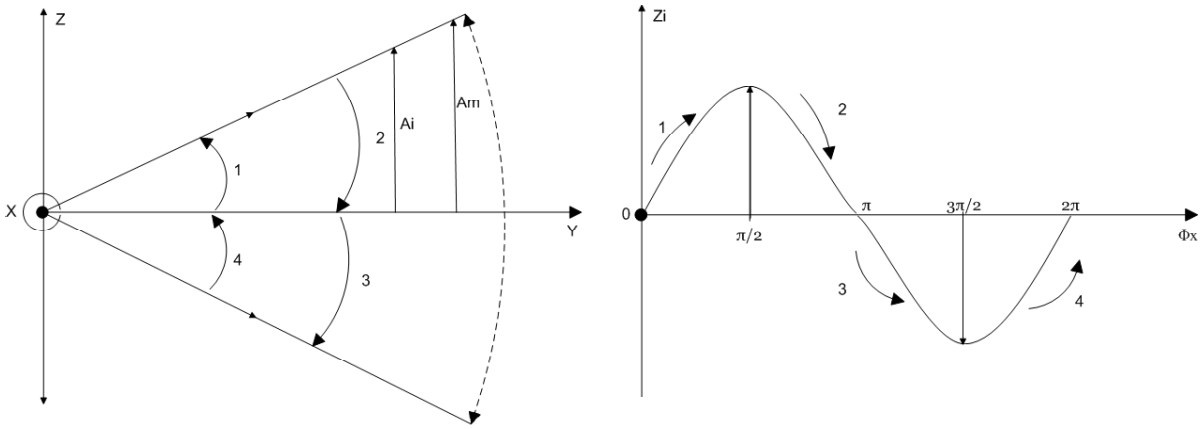

Figure 1. The wing flapping pattern

Here $-\vec{V}$ is the surface velocity and $\vec{n} = \vec{n}(X, Y, Z, t)$ is the vector normal to this moving surface as viewed from the inertial frame of reference. Note that $\vec{V}$ is defined with the minus sign so that the undisturbed flow velocity will be positive in the body's frame of reference.

Since Eq. (3) does not depend directly on time, the time dependency is introduced through this boundary condition. Thus, the location and orientation of $\vec{n}$ can vary with time.

The second boundary condition requires that the flow disturbance due to the body's motion through the fluid diminish far from the body:

$$\lim_{|\vec{R}-\vec{R}_0|\to 0} \vec{\nabla}\Phi = \vec{0} \tag{5}$$

where $\vec{R} = (X, Y, Z)$.

The mathematical problem is described schematically in Figure 3. Laplace's equation for the velocity potential must be solved for an arbitrary body with boundary S_B enclosed in a volume $\mathbf{V}$ with the outer boundary S_∞. The boundary conditions (4) and (5) apply to S_B and S_∞, respectively. The normal vector $\vec{n}$ is defined such that it always points outside the region of interest $\mathbf{V}$.

Using one of Green's identities, for two scalar functions of position Φ_1 and Φ_2 we have:

$$\int_S (\Phi_1 \nabla\Phi_2 - \Phi_2 \nabla\Phi_1)\cdot \vec{n} dS = \int_V (\Phi_1 \nabla^2\Phi_2 - \Phi_2 \nabla^2\Phi_1) dV \tag{6}$$

Here the surface integral is taken over the boundaries S, including a wake model S_W (which might model a surface across which a discontinuity in the velocity potential or the velocity may occur),

$$S = S_B + S_W + S_\infty \tag{7}$$

If Φ is the potential of the flow of interest in $\mathbf{V}$, and r is the distance from a point $P(x, y, z)$, as shown in Figure 3, by substituting $\Phi_1 = 1/r$ and $\Phi_2 = \Phi$, the above identity can be expressed as:

$$\vec{\nabla}\Phi = \vec{\nabla}\Phi_\infty - \frac{1}{4\pi}\int_{S_B} \sigma\vec{\nabla}(\frac{1}{r})dS + \frac{1}{4\pi}\int_{S_B, S_W} \mu\vec{\nabla}[\frac{\partial}{\partial n}(\frac{1}{r})]dS \tag{8}$$

where σ and μ are source and doublet strengths, respectively and Φ_∞ refers to the free stream potential. As mentioned before, source-sink and doublet singularity elements are used on the solid body surface. Only doublet singularity is used for wake. In this relation, $\partial/\partial n$ represents derivative in normal direction to the body's surface. This derivative for the doublet indicates the orientation of the element. According to this equation, the singularity elements induce potential Φ at a point which is located in distance r from them. Using the Dirichlet boundary condition, this integral equation is reduced below into algebraic form for the body and wake panels:

$$\sum_{k=1}^{N} C_k\mu_k + \sum_{l=1}^{N_w} C_l\mu_l + \sum_{k=1}^{N} B_k\sigma_k = 0 \tag{9}$$

where N and N_w are numbers of body and wake panels respectively. In this relation, source strengths are known through setting the condition of zero normal velocity at each body panel (relation (7)). The coefficients B_k and C_k can be found by double integration of distribution functions of source and doublet singularities on each panel. If a surface element with a constant-strength source distribution σ per area bound by four straight lines is considered, then the potential at an arbitrary point $P(x, y, z)$ due to this element is :

$$\Phi(x, y, z) = -\frac{\sigma}{4\pi}\int_S \frac{dS}{\sqrt{(x-x_0)^2 + (y-y_0)^2 + z^2}} \tag{10}$$

where $(x_0, y_0, 0)$ is the coordinates of each corner points of the element. Similarly for a constant strength

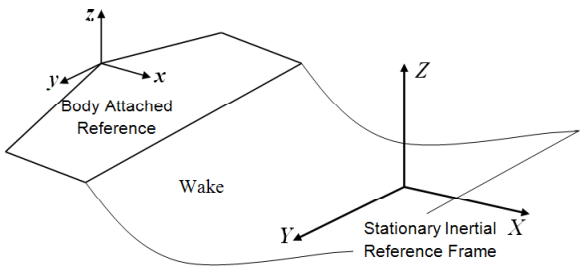

Figure 2. Inertial and non-inertial reference frames.

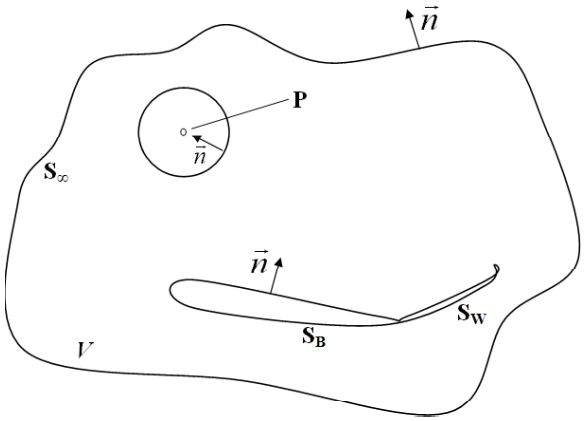

Figure 3. Nomenclature used to define the potential flow problem.

doublet distribution μ per area, the potential at an arbitrary point $P(x,y,z)$ is:

$$\Phi(x,y,z) = \frac{-\mu}{4\pi} \int_S \frac{zdS}{[(x-x_0)^2+(y-y_0)^2+z^2]^{3/2}} \tag{11}$$

For the sake of simplicity, only constant strength doublet and source panels are used. To solve Eq. (8) for the flapping wings in a non-inertial reference frame, time derivatives must be converted between inertial and moving coordinate systems through the following equation:

$$(\frac{\partial}{\partial t})_{inertial} = (\frac{\partial}{\partial t})_{body} - [\vec{V}_0 + \vec{V}_{rel} + \vec{\Omega} \times \vec{r}] \cdot (\frac{\partial}{\partial x}, \frac{\partial}{\partial y}, \frac{\partial}{\partial z}) \tag{12}$$

In addition, it is necessary to transform coordinates as well as velocity components from the inertial to the body reference system and vice versa. This is done by using the rotation tensor $\tilde{Q}$, which is function of the momentary rotation angles (in each direction).

$$\vec{P}_{Inertial} = \tilde{Q}\vec{P}_{Body} \tag{13}$$

$$\tilde{Q} = \begin{bmatrix} \cos(\psi(t)) & \sin(\psi(t)) & 0 \\ -\sin(\psi(t)) & \cos(\psi(t)) & 0 \\ 0 & 0 & 1 \end{bmatrix} \begin{bmatrix} \cos(\theta(t)) & 0 & -\sin(\theta(t)) \\ 0 & 1 & 0 \\ \sin(\theta(t)) & 0 & \cos(\theta(t)) \end{bmatrix} \begin{bmatrix} 1 & 0 & 0 \\ 0 & \cos(\gamma(t)) & \sin(\gamma(t)) \\ 0 & -\sin(\gamma(t)) & \cos(\gamma(t)) \end{bmatrix} \tag{14}$$

where $\psi(t)$, $\theta(t)$, $\gamma(t)$ are sideslip, attack and roll angles at a specified time, respectively.

It is possible to transform Eqs. (3) and (4) into the body's frame of reference without explicitly knowing $\tilde{Q}$. As at any moment, the continuity equation is independent of the coordinate system orientation, and the mass should be conserved. Therefore, the quantity $\nabla^2\Phi$ is independent of the instantaneous coordinate system, and the continuity equation in terms of (x,y,z) remains unchanged.

Also two boundary conditions (4) and (5) should state the same physical conditions. The gradient $\vec{\nabla}\Phi$ will have the same magnitude and the kinematic velocity $\vec{V}$ is given by the Eq. (15):

$$\vec{V} = \vec{V}_0 + \vec{V}_{rel} + \vec{\omega} \times \vec{r} \tag{15}$$

Therefore, the zero-velocity normal to a solid surface boundary, in the body frame, results in the sources strengths of body panels:

$$\sigma = -(\vec{V}_0 + \vec{V}_{rel} + \vec{\omega} \times \vec{r}) \cdot \vec{n} \tag{16}$$

where $\vec{V}_0$ and $\vec{\omega}$ are translational and rotational velocities of the moving body with respect to the inertial reference frame. The parameter $\vec{V}_{rel}$ refers to the velocity of moving parts of the body with respect to the body-attached coordinate system. Due to the flapping movement, there is a rotational motion in x-direction. In each time step, by solving a set of Eq. (9), doublet strengths of the body panels are determined.

The above mathematical formulation, even after selecting a desirable combination of sources and doublets and after fulfilling the boundary conditions on the body surface, is not unique. For lifting flow conditions, the magnitude of circulation depends on the wake shape and the location of the wake shedding line; therefore, an appropriate wake model needs to be established. The wake model can be based on two physical considerations:

- a) Wake Strength: The simplest solution to this problem is to apply the two-dimensional Kutta condition along the trailing edge (TE) of the lifting wing. If circulation is modeled by a vortex distribution γ, then:

$$\gamma_{TE} = 0 \tag{17}$$

The validity of this assumption depends on the component of kinematic velocity normal to the trailing edge, which must be much smaller than the characteristic velocity (e.g.,V_{ref}) for Eq. (17) to be valid. Also, the Kelvin condition can be used to calculate the change in the wake circulation:

$$\frac{d\Gamma}{dt} = 0 \tag{18}$$

- b) Wake Shape: Following this requirement that the wake is force free, the Kutta-Joukowski theorem states that for the wake, the velocity should be parallel to the circulation vector.

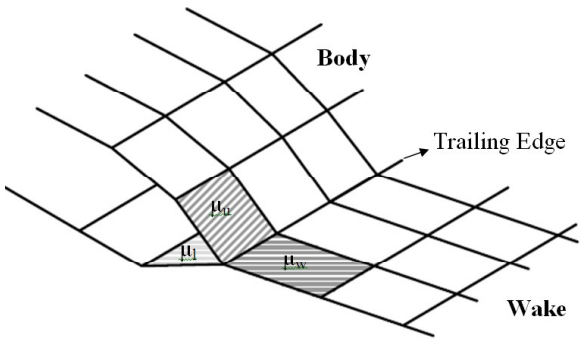

Figure 4. Wake shedding procedure

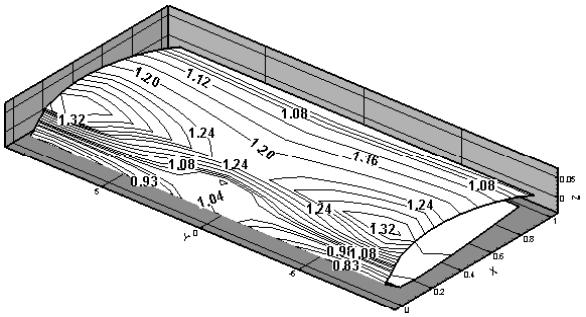

(a) Phase = 0 deg.

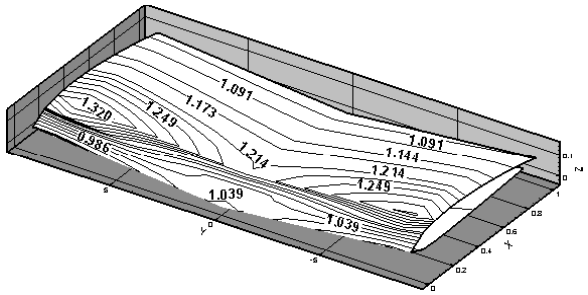

(b) Phase = 30 deg.

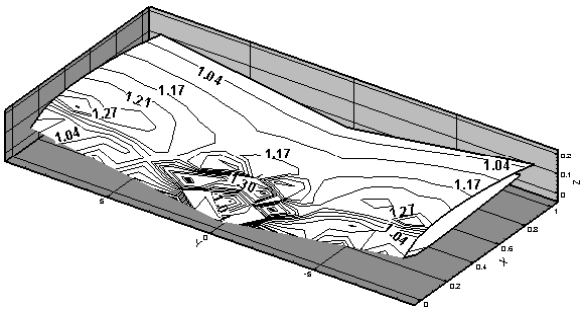

(c) Phase = 60 deg.

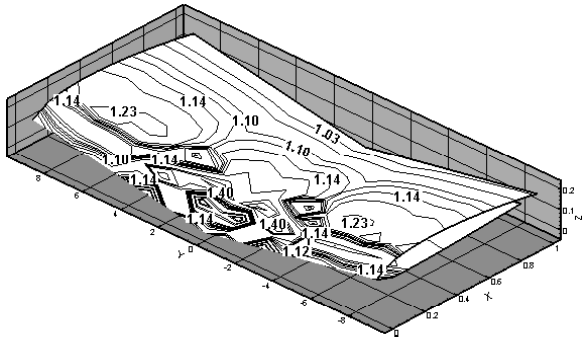

(d) Phase = 90 deg.

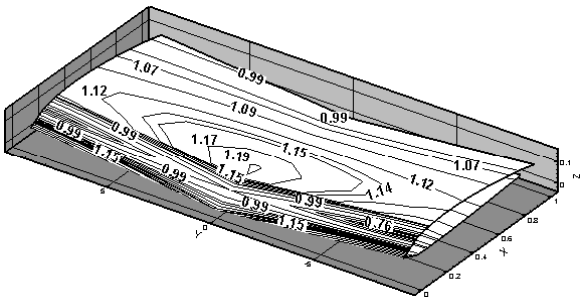

(e) Phase = 150 deg.

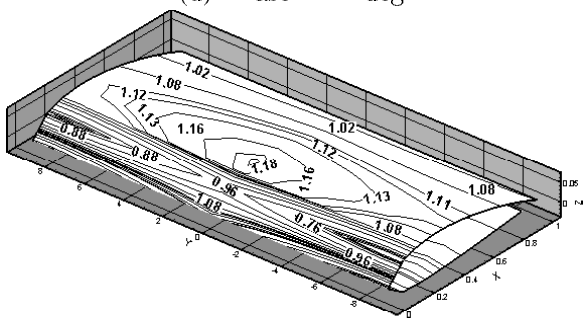

(f) Phase = 180 deg.

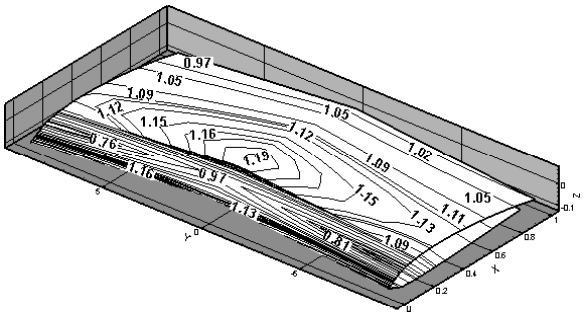

(g) Phase = 210 deg.

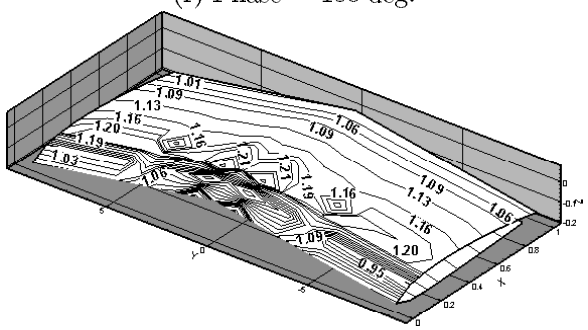

(h) Phase = 270 deg.

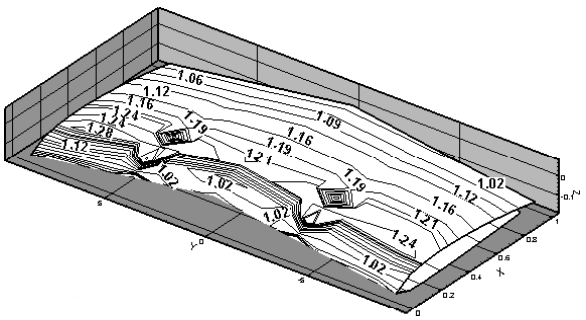

(i) Phase = 300 deg.

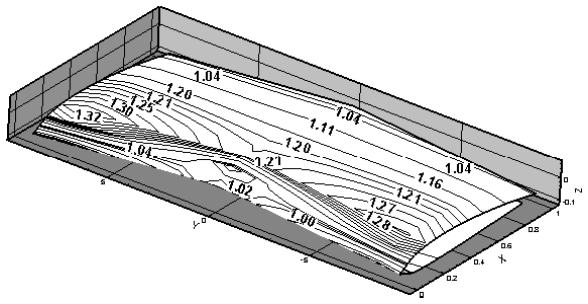

(j) Phase = 330 deg.

Figure 5. Velocity contours in different flapping phase angles for $\frac{\omega A_m}{V}$ =0.018.

The wake shedding procedure is described schematically in Figure 4. A typical trailing edge segment is shown with momentary upper μ_u and lower μ_l doublet strengths. The Kutta condition requires that the vorticity at the trailing edge remain zero:

$$\mu_w = (\mu_u - \mu_l)_{TE} \tag{19}$$

Thus, the strength of the latest wake panel μ_w is directly related to the wing's unknown doublets.

At the end of each time step, wake roll up is done. Since the wake is force free, each wake panel must move at the local stream velocity, which is equal to the total induced velocity at each wake corner point calculated in the stationary inertial frame.

After finding the distribution of singularities on the body and wake in a specified time step, the aerodynamic calculation is done. At first, the total velocity in each body panel is found by adding the kinematic and induced (perturbation) velocity components. The induced velocity components are obtained by derivation of doublet and source potential functions in the local coordinate system of each panel. The pressure coefficient can now be computed for each panel as:

$$C_P = \frac{P - P_\infty}{(1/2)\rho V_{ref}^2} = -\frac{(\vec{\nabla}\Phi)^2}{V_{ref}^2} + \frac{2}{V_{ref}^2}(\vec{V}_0 + \vec{V}_{rel} + \vec{\omega} \times \vec{r}) \cdot \vec{\nabla}\Phi - \frac{2}{V_{ref}^2}\frac{\partial \Phi}{\partial t} \tag{20}$$

The contribution of an element with an area of ΔS_k to the aerodynamic load $\Delta \vec{F}_k$ is:

$$\Delta \vec{F}_k = -Cp_k \, (\frac{1}{2}\rho V_{ref}^2)_k \, \Delta S_k \, \vec{n}_k \tag{21}$$

To perform the aerodynamic analysis of the flapping wings, a general unsteady, three-dimensional panel method computer code has been specifically developed for this study. Among the basic wing geometries, the rectangular wings are used in the present study. In the kinematic modeling, the orientation of wing in each time step is determined in correspondence to the flapping condition. A complete flapping cycle consists of two upstroke and downstroke levels and its duration depends on the flapping frequency. In our study, only the effect of right and left wings is considered. Both right and left wings flap symmetrically with respect to the wing-root.

RESULTS

A rectangular wing with NACA2410 airfoil is considered here (except in the last results at which NACA2412 is also used). To perform a non-dimensional analysis, the chord length of the airfoil, the

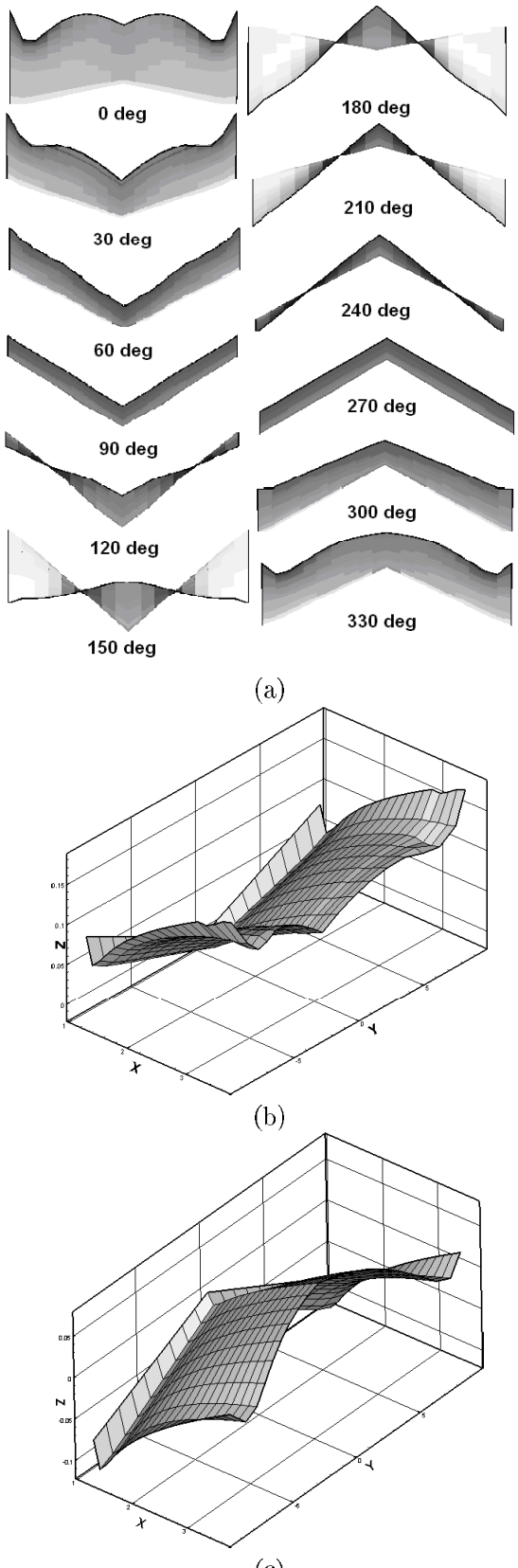

Figure 6. (a) Back view of trailing edge wake in different flapping phase angles for $\frac{\omega A_m}{V}$ =0.018, (b) Wake at phase angle 30 degrees for NACA2410 wing, (c) Wake at phase angle 330 degrees for NACA2410 wing.

translational kinematic velocity and the fluid density are assumed to be unity. For different values of the length of the flapping stroke (A_m in Figure 1), the rotational speed, the angle of attack and the wing-span length, there are distinct findings. To study the effects of the above-mentioned parameters on the aerodynamic design coefficients, the other parameters are assumed to be constant. For each set of these parameters, the flapping motion is repeated steadily as the time passes and translation continues unsteadily. After the time passes sufficiently, the aerodynamic design coefficients such as lift and pitching moment coefficients will be known. Additionally the wake of the flow which is separated from the trailing edge of the wing is obtained up to this time.

Velocity contours and wake shapes

The velocity contours at different flapping phase angles for a prescribed wing geometry and aerodynamic conditions are shown in Figure 5. In Figures 6-a, 6-b and 6-c, the back view schematic wake shape of the flow which is separated from the wing trailing edge during the time of different flapping phase angles is shown. These shapes are changed in each flapping phase.

The effect of the wing span on the chord ratio

In Figures 7(a-c), the distribution of lift, pressure drag and pitching moment coefficients are shown. For this set of diagrams, non-dimensional ratio $\omega A_m/V$ is equal to 0.18 (ω is the flapping frequency, A_m is the wing tip amplitude and V is the translational velocity) and the effect of parameter span on chord ratio is inspected. The diagrams of the lift and the pitching moment coefficients versus flapping phase angle seem to be harmonic but asymmetric. This asymmetry is due to the asymmetry of airfoil NACA 2410. In these figures, the wing starts to flap from a zero flapping phase angle. During the first part of upstroke (motion

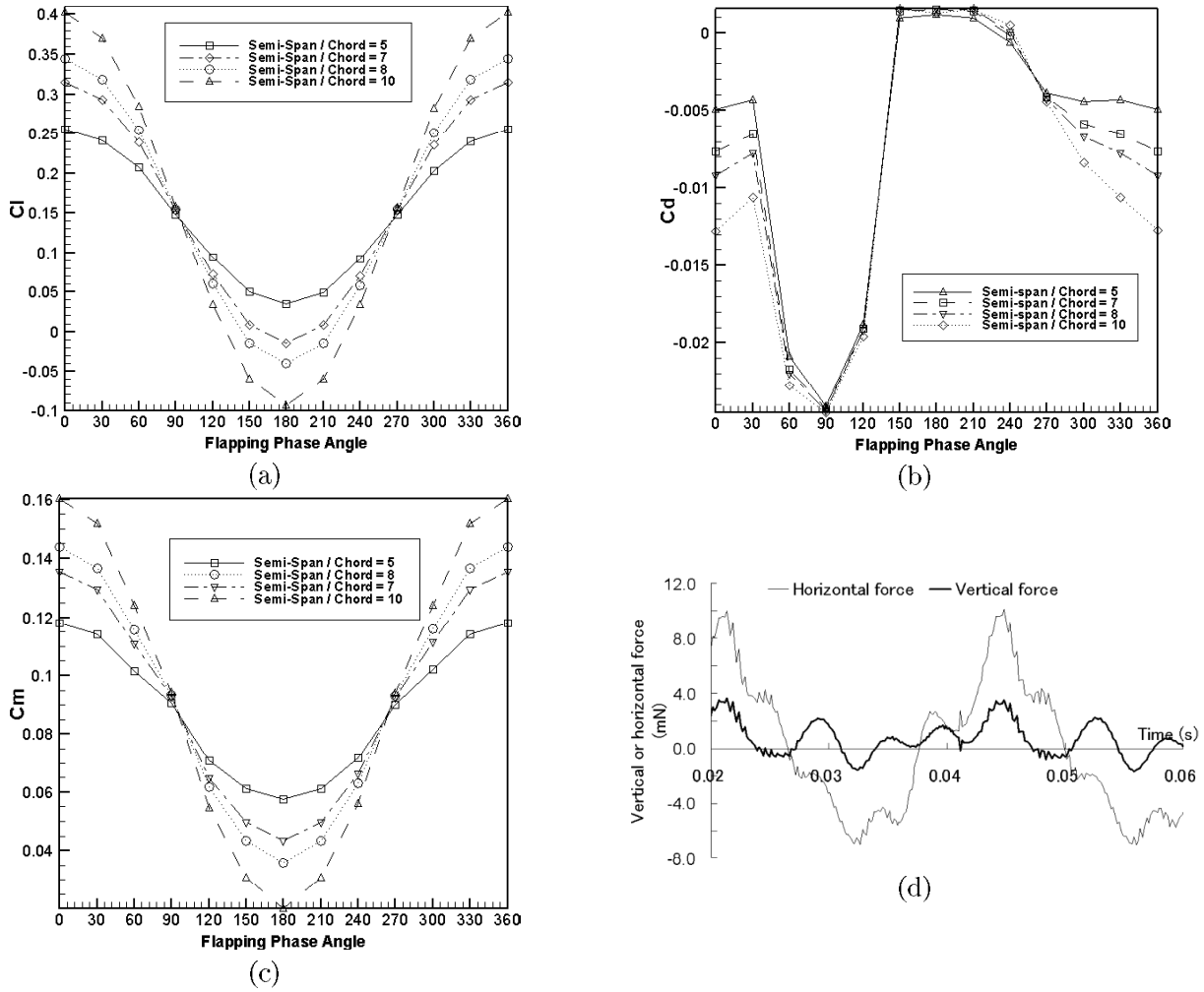

Figure 7. (a) Lift coefficient vs. flapping phase angle for different semi-span to chord ratios, (b) Drag coefficient vs. flapping phase angle for different semi-span to chord ratios, (c) Pitching moment coefficient vs. flapping phase angle for different semi-span to chord ratio, (d) Vertical and horizontal forces of a two-dimensional flapping airfoil from [9].

1 in Figure 1), phase angle changes from zero to 90 degrees. For this part of motion, the lift, the drag and the pitching moment decreases. At phase angle of 90 degrees, the diagrams of different values of the span to chord ratios have the same values. The decreasing of C_l (the lift coefficient) and C_m (the pitching moment coefficient) continues for phases between 90 and 180 degrees (in the first half of downstroke), until the minimum values are reached at the end of the first half of the downstroke. At this phase, both halves of the wing are in a flat orientation and the flapping velocity is maximum negative in relation 2. In the second parts of the downstroke and upstroke (the motions 3 and 4 in Figure 1, respectively), both C_l and C_m increase. It is not surprising that the lift and drag coefficients experience negative values. Because of the motion of the wing in negative Z direction, the normal vectors of the panels on the wing surface are in the negative direction. Therefore, the lift and the pressure drag forces are totally positive. To compute the values of the total lift and drag forces as well as the pitching moment, the distribution of lift, drag and moment must be integrated, respectively in relation to the flapping phase angle. To reach the total force and moment in a specified time step, the corresponding values at each time step must be added. According to this criterion and the diagrams in Figure 7, more lift force is produced if the wing span to chord ratio increases. But this achievement is expensive because when the wing span increases, the flapping wing structure experiences

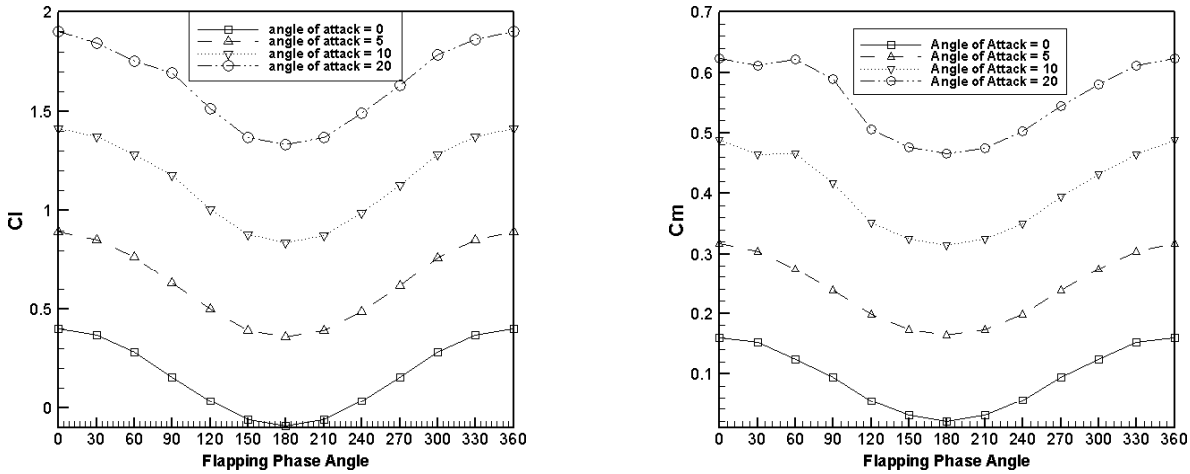

(a) (b)

Figure 8. (a) Lift coefficient vs. flapping phase angle for different angles of attack, (b) Pitching moment coefficient vs. flapping phase angle for different angles of attack.

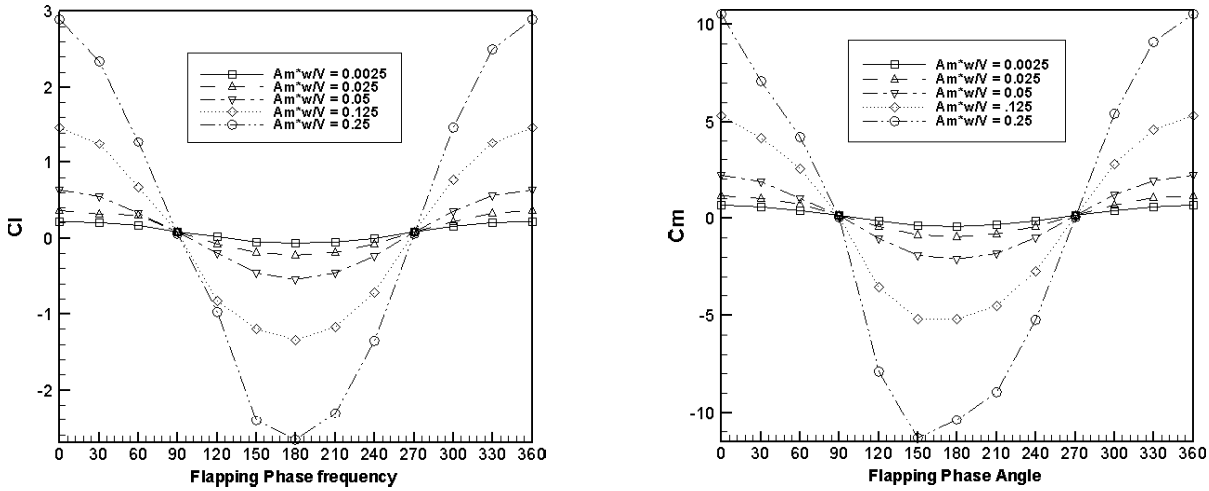

(a) (b)

Figure 9. (a) Lift coefficient vs. flapping phase angle for different $\omega A_m/V$, (b) Pitching moment coefficient vs. flapping phase angle for different $\omega A_m/V$.

extended values of moment. This moment is periodic and enforces consideration of the fatigue phenomenon in the structure design. Figure 7-d shows the vertical and horizontal forces of a two-dimensional flapping airfoil obtained by Hamamoto et. al., 2007 [9], which demonstrates good agreement with the results of this study, Figures 7-a and 7-b. The differences of the Figures are due to the three-dimensional analysis of the present work.

The effect of the angle of attack

In Figures 8-a and 8-b, the lift and the moment coefficients are depicted versus phase angle for different values of angles of attack. In these diagrams, the wing span to chord ratio $\omega A_m/V$, and the semi-span to chord ratio are set to be fixed. As expected, by increasing the angle of attack, both C_l and C_m increase too. In addition, the harmonic shapes of C_l and $_m$ diagrams versus flapping phase angle are closely preserved. At higher angles of attack, asymmetry of the C_l and C_m diagram is more visible. It is interesting that the difference between the maximum and minimum values of the C_l and C_m is approximately the same for each diagram.

The effect of the flapping frequency

In Figures 9-a and 9-b, the effects of the flapping frequency (ω) are investigated. As shown in these figures, by increasing the ratio $\omega A_m/V$, the differences between maximum and minimum values of the lift and moment coefficients increase as well. Therefore, for a specified ratio $\omega A_m/V$, that is, a specified wing geometry, as well as specific translational velocity and flapping amplitude (A_m), faster flapping ends in more lift force. But this advantage is accompanied with higher moments. In addition, the effect of asymmetry of the cross sectional airfoil is more important in higher flapping frequencies.

The effect of the flapping amplitude

At last, as shown in figures 10-a and 10-b, aerodynamic design coefficients have the minimum sensitivity to the parameter of wing tip flapping amplitude (A_m). The sensitivity of design coefficients to this parameter increases as this value increases. This means that to achieve higher values of C_l , it is better to change the other parameters such as wing to span ratio, the flapping frequency and the angle of attack.

The effect of wing section

In Figures 11-a to 11-c, lift, drag and moment coefficients of two wings with different cross airfoils (NACA2410 and NACA2412) are depicted against the flapping phase angle, for some values of $A_m\omega/V$. Approximately, the lift and moment coefficients of two wings are distributed in the same range, but these diagrams for NACA2412 (Figures 11a-c) are more asymmetric than NACA2410. Although the trend of drag coefficients diagrams of two wings are similar, the absolute values of these coefficients are higher for the NACA2412 wing.

CONCLUSION

A computer code based on the unsteady panel method has been developed to analyze the flapping wings. The prepared algorithm and the computer code are capable of modeling MAV's flapping wings in different unsteady conditions. The velocity contours on the wing and the trailing edge wake were shown for different conditions. Among the different effects, the influences of the wing

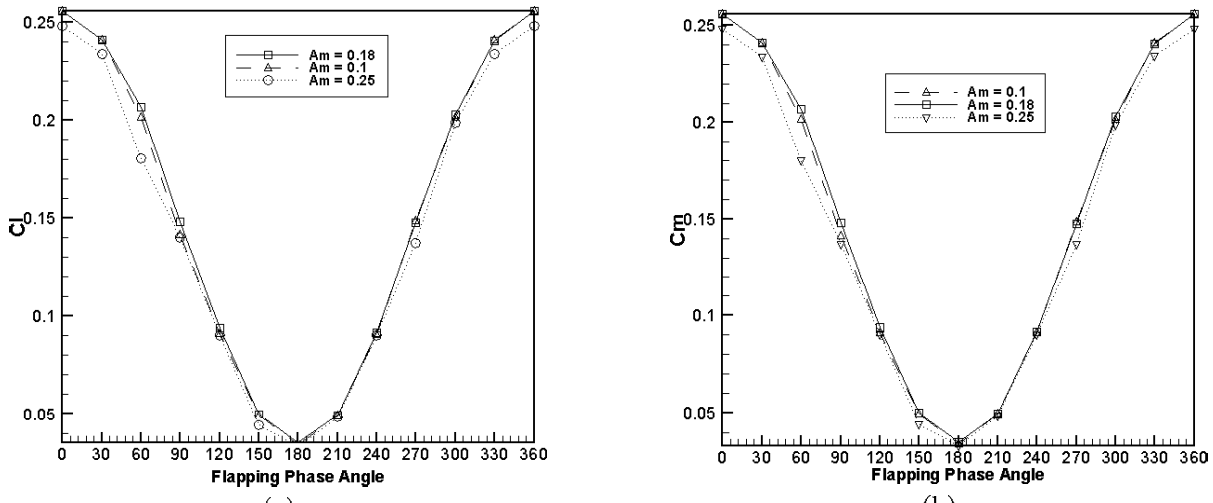

Figure 10. (a) Lift coefficient vs. flapping phase angle for different A_m, (b) Pitching moment coefficient vs. flapping phase angle for different A_m .

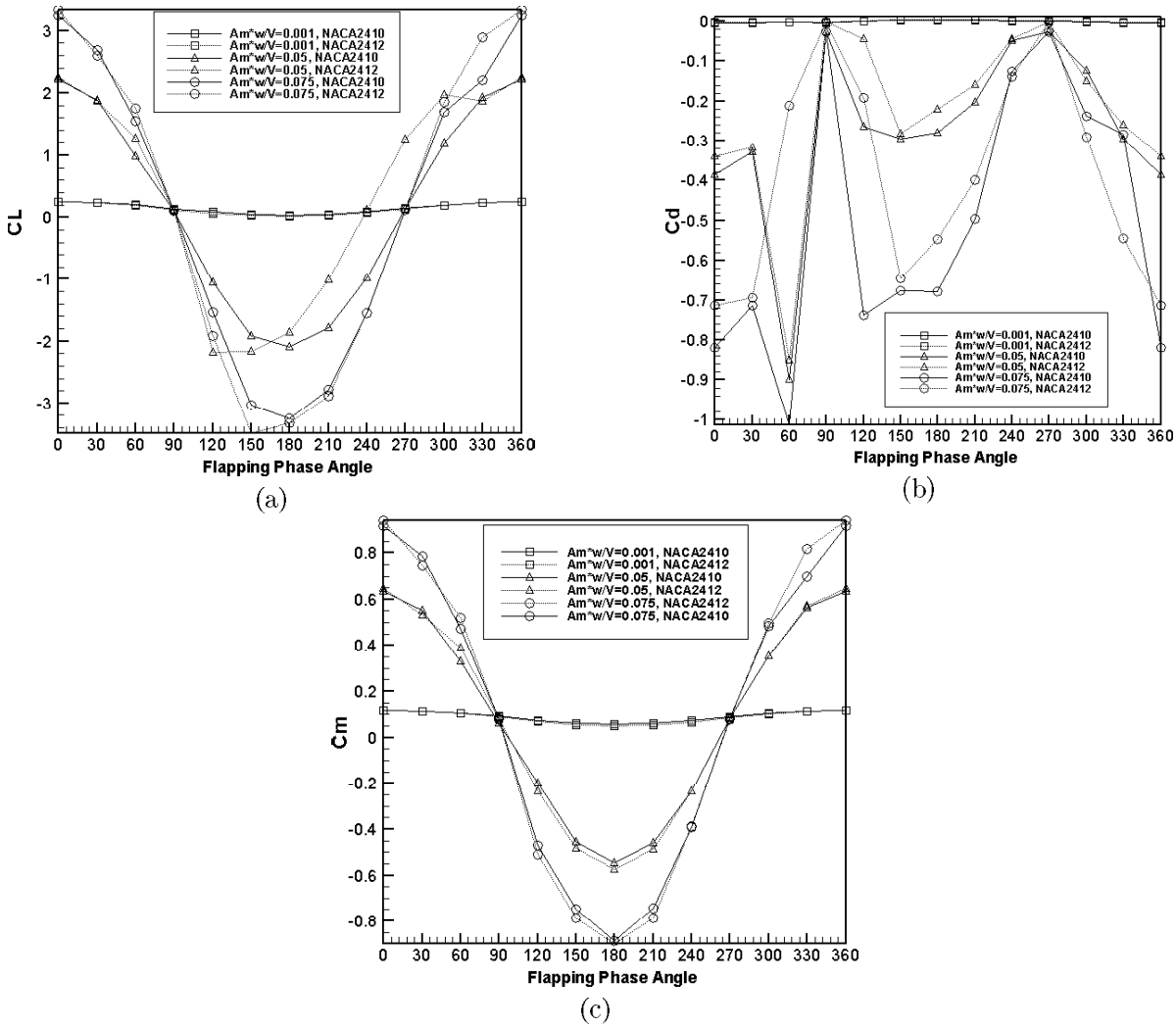

Figure 11. (a) Lift coefficient vs. flapping phase angle for NACA2410 and NACA2412 wings, (b) Drag coefficient vs. flapping phase angle for NACA2410 and NACA2412 wings, (c) Pitching moment coefficient vs. flapping phase angle for NACA2410 and NACA2412 wings.

span on chord ratio, the angle of attack, the flapping frequency and the wing section are studied. In each case, to investigate the effect of one parameter, the other ones were kept constant.

According to the results, more lift force is produced if the wing span to chord ratio or angle of attack or flapping frequency and flapping amplitude increases. However, this achievement is expensive; because in one or all of the mentioned conditions, the flapping wing structure experiences extended values of moment.

REFERENCES

1. Dial K.P., "An Inside Look at How Birds Fly: Experimental Studies of the Internal and External Processes Controlling Flight", *Report the Aerospace Profession, 38th Symposium Proceedings*, The Beverly Hilton, Beverly Hills, CA, (1994).
2. Kurtulus D.F., Davi L., Farcy A., Alemdaroglu N., "Aerodynamic Characteristics of Flapping Motion in Hover", *Journal of Experimental Fluids*, (2007).
3. Hamdani H., Sun M., "Aerodynamic Forces and Flow Structures of an Airfoil in Some Unsteady Motions at Small Reynolds Number", *Acta. Mechanic*, **145**, PP 173-187(2000).
4. Lai J., Platzer M.F., "Characteristics of a Plunging Airfoil at Zero Freestream Velocity", *Journal AIAA*, **39**, PP 531-534(2001).
5. Wang J.Z., Birch J.M, Dickinson M.H., "Unsteady Forces and Flows in Low Reynolds Number Hovering", *Journal of Experimental Biology*, **207**, PP 449-450(2004).
6. Dickinson M.H., "The Effects of Wing Rotation on Unsteady Aerodynamics Performance at Low Reynolds Numbers", *Journal of Experimental Biology*, **192**, PP 179-206(1994).

7. Smith M.J.C., Wilkin P.J. and Williams M.H., "The Advantages of an Unsteady Panel Method in Modeling the Aerodynamic Forces on Rigid Flapping Wings", *Journal of Experimental Biology*, **199**, PP 1073-1083(1996).

8. Katz J. and Plotkin A., *Low-Speed Aerodynamics, From Wing Theory to Panel Methods*, McGraw-Hill Inc., New York, (2001).

9. Hamamoto M., Ohata Y., Hara K., Hisada T., "Application of Fluid-Structure Interaction Analysis to Flapping Flight of Insects with Deformable Wings", *Journal of Advanced Robotics*, **21**(1-2), PP 1-2(2007).